PHYSICAL REVIEW B VOLUME 59, NUMBER 22 1 JUNE 1999-II

Structural and magnetic characterization of the frustrated triangular-lattice antiferromagnets $CsFe(SO_4)_2$ and $RbFe(SO_4)_2$

H. Serrano-González
School of Chemistry, University of Birmingham, Edgbaston, Birmingham B15 2TT, United Kingdom

S. T. Bramwell*
Department of Chemistry, University College London, Christopher Ingold Laboratories, 20 Gordon Street, London WC1H OAJ, United Kingdom

K. D. M. Harris* and B. M. Kariuki
School of Chemistry, University of Birmingham, Edgbaston, Birmingham B15 2TT, United Kingdom

L. Nixon and I. P. Parkin
Department of Chemistry, University College London, Christopher Ingold Laboratories, 20 Gordon Street, London WC1H OAJ, United Kingdom

C. Ritter
Institut Max von Laue–Paul Langevin, Boîte Postale 156, F-38042 Grenoble 09, France

(Received 7 October 1997; revised manuscript received 22 February 1999)

We describe the characterization, by magnetometry, neutron diffraction, and x-ray diffraction, of polycrystalline samples of $CsFe(SO_4)_2$ and $RbFe(SO_4)_2$. The crystal structures of these materials are of the trigonal $CsSb(PO_4)_2$ ($P\overline{3}$) type, in which the magnetic Fe^{3+} ions with spin $S=5/2$ occupy a triangular lattice in well-separated layers. Comparison of the low-temperature magnetic susceptibility with Monte Carlo simulation results shows that both compounds approximate very well to the two-dimensional Heisenberg model antiferromagnet on the triangular lattice. At the Néel temperatures, 4.4 K for $CsFe(SO_4)_2$ and 4.2 K for $RbFe(SO_4)_2$, the spins order three dimensionally, although this does not have a strong effect on the form of the susceptibility curve. The ordered magnetic structures have been determined for both materials, revealing that the spins form a three-sublattice structure in the basal plane, with adjacent spins rotated by 120° and with spins in alternate layers approximately antialigned. [S0163-1829(99)10121-8]

I. INTRODUCTION

Magnetic solids are said to be ‘‘frustrated’’ if there is no configuration of the atomic magnetic moments (spins) that simultaneously minimizes all the local interaction energies. There is continuing interest in such materials because they display a rich variety of behavior: spin glass ordering, incommensurate ordering, spin liquid ground states, chirality transitions, and new universality classes.[1]

The triangular-lattice antiferromagnet is the simplest two-dimensional frustrated system.[2] It exhibits a wealth of unusual properties, which despite extensive study are still only poorly understood. These include unusual critical exponents,[3] unusual quantum fluctuation effects,[4] and anomalous percolation properties.[5] The properties of the triangular-lattice antiferromagnet arise from the combination of frustration with low dimensionality, and they depend critically on the spin value and anisotropy. With Ising spins, the zero-temperature ground state has power-law decay of correlations;[6] with classical *XY* or Heisenberg spins, a three-sublattice ordered structure is adopted, but with a defect-mediated transition at higher temperature.[2] Anderson speculated that the quantum (spin $S=1/2$) Heisenberg model on a triangular lattice has disordered ‘‘spin liquid’’ ground state and went on to propose that a doped version of this model would be a high-temperature superconductor.[7] Although it is now thought that the undoped model has weak conventional order, it is clear that quantum fluctuations are particularly important in this system.[8]

Good experimental realizations of the two-dimensional triangular-lattice antiferromagnet are relatively few, the main examples being the vanadium dihalides[9] and delafossite-type oxides.[10] In contrast, the three-dimensional (‘‘stacked’’) triangular lattice is well represented by the ABX_3-type halides [e.g., $CsFeCl_3$ (Ref. 11)], which have been studied in great detail.[11,12] Quantum triangular-lattice antiferromagnets with spin $S=1/2$ are even rarer. $NaTiO_2$ (Ref. 13) and $LiNiO_2$ (Ref. 14) are possible candidates, but these have extended bonding and are poor model magnets. In a recent publication[15] we showed that the materials with layered crystal structures related to the mineral Yavapaiite $KFe(SO_4)_2$ (Ref. 16) are of interest as realizations of a model quasi-two-dimensional triangular-lattice antiferromagnet. This series of materials is particularly notable for its chemical versatility,

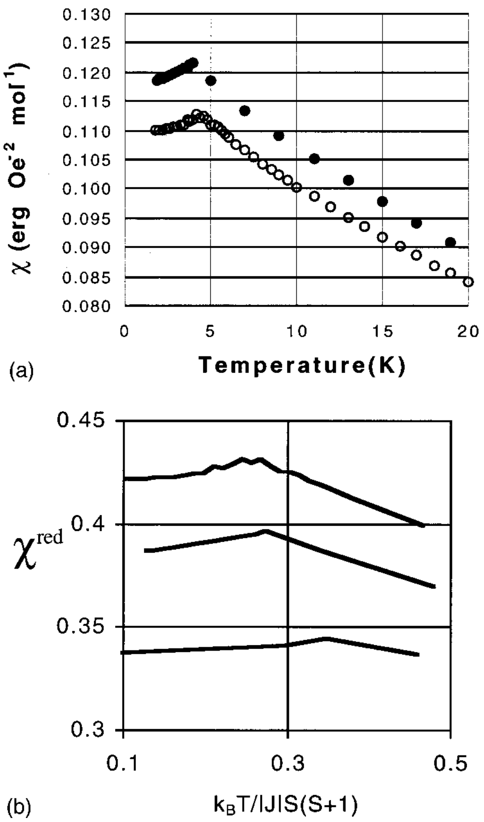

FIG. 1. (a) Magnetic susceptibility vs temperature for $CsFe(SO_4)_2$ (open circles) and $RbFe(SO_4)_2$ (solid circles). (b) Reduced susceptibility (defined in the text) vs reduced temperature for $CsFe(SO_4)_2$ (upper curve) and $RbFe(SO_4)_2$ (middle curve), compared with the Monte Carlo data of Fig. 14, Ref. 2 (lower curve).

and we can realize both quantum and quasiclassical systems by using $M=\mathrm{Ti}$ ($S=1/2$) and Fe ($S=5/2$), respectively.

In general, the Yavapaiite family can be described by the formula $AM(XO_4)_2$, in which A is a univalent (e.g., Na^+) or divalent (e.g., Ba^{2+}) cation, M is a trivalent (e.g., Fe^{3+}) or tetravalent (e.g., Mo^{4+}) cation, and XO_4 is a divalent (e.g., $SO_4{}^{2-}$) or trivalent (e.g., $PO_4{}^{3-}$) oxy-anion. Subject to the requirement of charge balance, practically any combination of such species can be realized.[16] In the general structure type, the M ions lie in triangular arrays in well-separated layers formed by the XO_4 groups, and the A ions occupy the interlayer space. The $AM(XO_4)_2$ phases characterized so far can be classified into six structure types, which differ in the symmetry of the layers and in the way that these layers are stacked.[16] In $CsFe(SO_4)_2$ and $RbFe(SO_4)_2$, the layers are constructed from FeO_6 octahedra and SO_4 tetrahedra, linked via vertices such that each octahedron is linked to six tetrahedra and each tetrahedron is linked to three octahedra. The fourth vertex of each tetrahedron is not shared in this way and points into the interlayer space. The magnetic properties of the Yavapaiite materials can be classified into two major groups, depending on the symmetry of the triangular net occupied by the magnetic atoms. The materials in the first group, which includes $CsFe(SO_4)_2$ and $RbFe(SO_4)_2$, have an equilateral triangular lattice, whereas those in the second group, which includes $KFe(SO_4)_2$ and $NaFe(SO_4)_2$, have an isoceles triangular (i.e., centered rectangular) lattice. While the latter materials are of interest as realizations of the so-called ''row model,''[17] the current paper focuses on those with the undistorted triangular lattice: $CsFe(SO_4)_2$ and $RbFe(SO_4)_2$. On account of the large interlayer spacing of these materials and the ^6S ground term of Fe^{3+}, they would be expected to approximate the two-dimensional Heisenberg antiferromagnet on the triangular lattice.

In this paper, we describe the structural and magnetic characterization of polycrystalline samples of $CsFe(SO_4)_2$ and $RbFe(SO_4)_2$, using powder x-ray diffraction (both synchrotron and laboratory sources), powder neutron diffraction, and magnetometry. Section II describes the synthesis of the samples, and Sec. III describes magnetic susceptibility measurements between 1.8 and 300 K, which are analyzed to give exchange constants and compared to the results of Monte Carlo simulations.[2] Section IV describes the x-ray diffraction and neutron diffraction experiments. In Sec. IV C we report the crystal structures of $CsFe(SO_4)_2$ and $RbFe(SO_4)_2$, both at ambient temperature and low temperature, determined from Rietveld refinement of x-ray and neutron powder diffraction data, respectively. Section IV E then describes the magnetic structure determination for both materials using neutron diffraction data in the range 1.3–10 K. Conclusions are drawn in Sec. V.

II. PREPARATION OF SAMPLES

All reagents were purchased from Aldrich Chemical Co. and were used as supplied. All solvents were degassed with dinitrogen prior to use. Cesium sulfate or rubidium sulfate (8.3 mmol) and iron (III) sulfate pentahydrate (8.3 mmol) were added to distilled water (40 ml). The solution was heated to 60 °C to dissolve the salts, allowed to cool to room temperature, and stirred for 24 h. During this period, an off-white solid precipitated. The solvent was removed under vaccum and the solid was ground with a pestle and mortar. The resulting solid was heated to 320 °C for 1 h, cooled to room temperature, reground, and further heated at 320 °C for 1 h. This heating and grinding cycle was found to give a

TABLE I. Results of fits to magnetic susceptibility (χ) data for $CsFe(SO_4)_2$ and $RbFe(SO_4)_2$. The Curie-Weiss constant θ and effective g factor g were from plots of $1/\chi$ vs temperature in the range 35–100 K. The exchange constant J (assuming six nearest neighbors) and the magnetic moment $\mu=g\sqrt{\{S(S+1)\}}$ were determined from the fitted values of θ and g, as described in the text. The effective moment μ_{eff} at 300 K is also listed.

Material	θ/K	$\{J/k_B\}/K$	g	μ/μ_B	μ_{eff}/μ_B
$CsFe(SO_4)_2$	−34.17(4)	−1.953(2)	2.019(9)	5.97(3)	5.48(1)
$RbFe(SO_4)_2$	−29.12(6)	−1.664(3)	2.010(1)	5.946(3)	5.73(1)

single-phase sample of good crystallinity. The materials prepared in this way were identified as $CsFe(SO_4)_2$ or $RbFe(SO_4)_2$ by x-ray powder diffraction, with d spacings found to match to literature values,[18] and energy-dispersive x-ray analysis (EDAX) (which showed uniform sample composition across many surface spots with the required cesium, rubidium, iron, and sulfur ratios).

For this sample characterization, the powder x-ray diffraction patterns were measured with a Siemens D5000 diffractometer using germanium monochromated Cu $K\alpha_1$ radiation ($\lambda = 1.5406$ Å); scanning electron microscopy (SEM) and EDAX were conducted on a Hitachi S-4000 scanning electron microscope. Sample heating was carried out in a Lenton Thermal Designs tube furnace (heating and cooling rates were about 5 °C per minute).

III. MAGNETIC SUSCEPTIBILITY

A. Experimental details

Magnetic susceptibilities were measured in the temperature range 1.8–300 K using a Quantum Design superconducting quantum interference device (SQUID) magnetometer at the Royal Institution of Great Britain. Samples of mass 42.57 mg $[CsFe(SO_4)_2]$ and 20.69 mg $[RbFe(SO_4)_2]$ were mounted in a gel capsule contained in a uniform plastic cylinder. Identical gel capsules positioned above and below the sample ensured a uniform magnetic environment. Each reported measurement was the average of several readings, with the standard deviation in each set of readings a factor of about 10^{-4} of the measured moment. A magnetic field $\mathbf{H}$ of 500 Oe was applied to the sample, and measured magnetizations per unit mass $\boldsymbol{\sigma}$ (erg $\mathrm{Oe^{-1}\,g^{-1}}$) were converted to molar susceptibilities χ (erg $\mathrm{Oe^{-2}\,mol^{-1}}$) using $\chi = \sigma m/H$, where m is the theoretical molar mass ($\mathrm{g\,mol^{-1}}$). The diamagnetic correction arising from the sample was estimated to be negligible.

B. Results and discussion

The magnetic susceptibility χ versus temperature graphs for $CsFe(SO_4)_2$ and $RbFe(SO_4)_2$ are plotted in Fig. 1(a); a weak cusp is observed in the susceptibility at $T = 4.4(2)$ K for $CsFe(SO_4)_2$ and 4.2(2) K for $RbFe(SO_4)_2$. In order to estimate an exchange constant, the magnetic data were transformed into inverse magnetic susceptibility $1/\chi$ versus temperature T and analyzed by linear regression in the temperature range 35–100 K according to the Curie-Weiss law using

$$\frac{1}{\chi} = \frac{T}{C} - \frac{\theta}{C}, \tag{1}$$

with

$$C = \frac{Ng^2\mu_B^2 S(S+1)}{3k_B}, \quad S = \frac{5}{2}. \tag{2}$$

The results of the fits, taking the effective g value g and the Curie-Weiss constant θ as the adjustable parameters, are given in Table I. Both the magnetic moment $\mu = g\mu_B\sqrt{[S(S+1)]}$ and the effective moment $\mu_{\mathrm{eff}} = \sqrt{(8\chi T)}$ measured at 300 K (see Table I) are close to the expected value 5.92 for the ^{6}S state of Fe^{3+}. The Curie-Weiss constant was further analyzed by the equation

$$\theta = (1/3)zJS(S+1) \tag{3}$$

to give an effective near-neighbor exchange constant J, assuming six nearest neighbors (i.e., $z = 6$). These are also listed in Table I. This assumption neglects the contribution from further neighbor exchange pathways and is likely to be a good approximation for $CsFe(SO_4)_2$ and $RbFe(SO_4)_2$ on account of the large second-nearest-neighbor separation (about 8 Å). The exchange constant J so defined is appropriate to the spin Hamiltonian

$$H = J\sum_{\langle ij\rangle} \mathbf{S}_i \cdot \mathbf{S}_j, \tag{4}$$

where the sum is defined such that each bond is counted once and thus corresponds to the definition used by Kawamura and Myashita[2] in their Monte Carlo study of the classical Heisenberg antiferromagnet on the triangular lattice. To facilitate comparison with the Monte Carlo data, we define a reduced magnetic susceptibility χ^{red} and reduced temperature T^{red}, which can be directly compared to the quantities used in the Monte Carlo simulations. χ^{red} is a dimensionless quantity defined as

$$\chi^{\mathrm{red}} = \frac{\chi|J|}{Ng^2\mu_B^2/3}, \tag{5}$$

and T^{red} is defined as

$$T^{\mathrm{red}} = \frac{k_B T}{|J|S(S+1)}. \tag{6}$$

The reduced susceptibility versus temperature for both $CsFe(SO_4)_2$ and $RbFe(SO_4)_2$ is shown in Fig. 1(b) in the region of the cusp. For both materials, the susceptibility curve is very similar to that observed in the Monte Carlo simulations.[2] For $CsFe(SO_4)_2$ the cusp occurs at $T_c^{\mathrm{red}} = 0.25$, $\chi_c^{\mathrm{red}} = 0.43$, and for $RbFe(SO_4)_2$ it occurs at $T_c^{\mathrm{red}} = 0.29$, $\chi_c^{\mathrm{red}} = 0.4$, which may be compared to the classical simulation result (Fig. 14 of Ref. 3) $T_c = 0.33$, $\chi_c = 0.35$. In $CsFe(SO_4)_2$ and $RbFe(SO_4)_2$, the cusp in fact marks a three-dimensional ordering transition (see Sec. IV), but the similarity between experiment and Monte Carlo simulation suggests that three-dimensional fluctuations do not have a significant effect on the behavior of the uniform susceptibility. This is expected for a layered magnet with very weak interlayer coupling, as two-dimensional fluctuations dominate the thermal behavior both above and below the three-dimensional ordering temperature.[19,20] The effect of three-dimensional fluctuations is expected to be confined to a small temperature range near the ordering temperature and then, principally, only at the ordering wave vector; so in the case of an antiferromagnet, the uniform susceptibility is particularly insensitive to three-dimensional effects, although these are likely to cause a small shift in transition temperature from the purely two-dimensional case. In the present study, the difference between the experimental susceptibility curve and that pre-

TABLE II. Structural parameters determined for $CsFe(SO_4)_2$ and $RbFe(SO_4)_2$: (a) $CsFe(SO_4)_2$ at ambient temperature [x-ray diffraction data, space group $P\overline{3}$, refined cell parameters $a=b=4.8807(1)$ Å, $c=8.7728(1)$ Å]. (b) $CsFe(SO_4)_2$ at 20 K [neutron diffraction data, space group $P\overline{3}$, refined cell parameters $a=b=4.8612(5)$ Å, $c=8.7081(1)$ Å]. (c) $RbFe(SO_4)_2$ at ambient temperature [x-ray diffraction data, space group $P\overline{3}$, refined cell parameters $a=b=4.8345(1)$ Å, $c=8.3068(4)$ Å]. (d) $RbFe(SO_4)_2$ at 8 K [neutron diffraction data, space group $P\overline{3}$, refined cell parameters $a=b=4.8189(5)$ Å, $c=8.2248(2)$ Å].

Atom	x/a	y/b	z/c	$U_{iso}/\text{Å}^2$
		(a)		
Cs	0	0	0	0.029(1)
Fe	0	0	1/2	0.027(1)
S	1/3	2/3	0.3094(9)	0.029(2)
O(1)	1/3	2/3	0.1417(9)	0.024(1)
O(2)	0.0851(16)	0.3558(9)	0.3638(7)	0.024(1)
		(b)		
Cs	0	0	0	
Fe	0	0	1/2	
S	1/3	2/3	0.3176(17)	
O(1)	1/3	2/3	0.1496(16)	
O(2)	0.1190(18)	0.3480(17)	0.3750(9)	
		(c)		
Rb	0	0	0	0.029(1)
Fe	0	0	1/2	0.036(1)
S	1/3	2/3	0.2997(4)	0.025(1)
O(1)	1/3	2/3	0.1225(4)	0.016(2)
O(2)	0.0852(17)	0.3504(10)	0.3554(7)	0.016(2)
		(d)		
Rb	0	0	0	
Fe	0	0	1/2	
S	1/3	2/3	0.3072(11)	
O(1)	1/3	2/3	0.1291(10)	
O(2)	0.1080(16)	0.3449(15)	0.3661(8)	

dicted by the Monte Carlo simulation is most likely to be due to quantum fluctuations in the real systems, although the effect of interlayer coupling might be manifest in the small differences in the cusp temperature and susceptibility between $CsFe(SO_4)_2$ and $RbFe(SO_4)_2$.

IV. DETERMINATION OF CRYSTAL STRUCTURES AND MAGNETIC STRUCTURES

A. Experimental details

X-ray powder diffractograms were recorded at ambient temperature on Station 2.3 at the Synchrotron Radiation Source, Daresbury Laboratory, U.K. The diffractograms were recorded in transmission geometry at wavelength $\lambda=1.2$ Å using a capillary sample holder. For $CsFe(SO_4)_2$, the data were recorded from $2\theta=5°$ to 80° in steps $\Delta(2\theta)=0.01°$ for a total data collection time of 7 h. For $RbFe(SO_4)_2$, the data were recorded from $2\theta=5°$ to 75° in steps $\Delta(2\theta)=0.02°$ for a total data collection time of 3.7 h. The high 2θ resolution of this instrument allowed unambiguous indexing of the diffractograms, although problems were encountered in the Rietveld refinement due to the fact that, with very high instrumental resolution, the line shape is dominated by sample-limited broadening. For this reason, x-ray powder diffractograms were recorded with lower instrumental resolution at ambient temperature on a Siemens D5000 diffractometer, operating in transmission mode with Ge-monochromatized Cu $K\alpha_1$ radiation and a linear position-sensitive detector covering 6° in 2θ. These diffractograms were recorded from $2\theta=10°$ to 80° in steps $\Delta(2\theta)=0.01°$ for a total data collection time of 12 h.

Neutron powder diffraction data were recorded using the medium-resolution high-flux powder diffractometer D1B at the Institut Laue-Langevin (ILL), Grenoble, France. This diffractometer is equipped with a position-sensitive detector covering an angular range of 80° in 2θ and composed of 400 elements separated by 0.2° in 2θ. The wavelength selected by the pyrolytic graphite monochromator was $\lambda=2.52$ Å. An ILL ''orange'' liquid helium cryostat was used to control temperature between 1.3 K and ambient temperature.

For determination of the low-temperature crystal structure, neutron powder diffractograms were recorded just above the Néel temperature (nuclear Bragg peaks), whereas for determination of the magnetic structure, neutron powder diffractograms were recorded below the Néel temperature (nuclear plus magnetic Bragg peaks). For $CsFe(SO_4)_2$ the data were recorded at 20 and 1.3 K, and for $RbFe(SO_4)_2$ the data were recorded at 8 and 1.3 K. Difference diffractograms, calculated by subtracting the diffractogram recorded above the Néel temperature from that recorded below the Néel temperature, contain peaks that arise from magnetic scattering only; the shifts in the positions of the nuclear peaks as a result of thermal lattice contraction on passing below the Néel temperature are negligible.

B. Data analysis

For determination of the crystal structure at ambient temperature, Rietveld refinement calculations were performed on the x-ray powder diffraction data using the GSAS program package.[21] The background points were fixed, and a pseudo-Voigt line shape function was used. To obtain satisfactory refinements, restraints (based on standard geometry) were applied to the S-O bond lengths and the O-S-O bond angles of the SO_4 tetrahedra.

In the early stages of refinement at ambient temperature, the isotropic atomic displacement parameters for all atoms were fixed at $U_{iso}=0.025\,\text{Å}^2$, whereas in the last stage of refinement the isotropic atomic displacement parameters were refined for all atoms, with the oxygen atoms constrained to have the same value.

For both $CsFe(SO_4)_2$ and $RbFe(SO_4)_2$, the refined crystal structure at ambient temperature (from x-ray powder diffraction data) was used as the starting model for refinement of the low-temperature nuclear structure, using neutron powder diffraction data recorded at a temperature of 20 K for $CsFe(SO_4)_2$ and 8 K for $RbFe(SO_4)_2$. In the refinement of the low-temperature nuclear structure, the atomic displacement parameters were fixed at zero in order to allow reliable determination of the scale factor.

The magnetic structure was determined using the difference neutron powder diffractogram calculated by subtracting

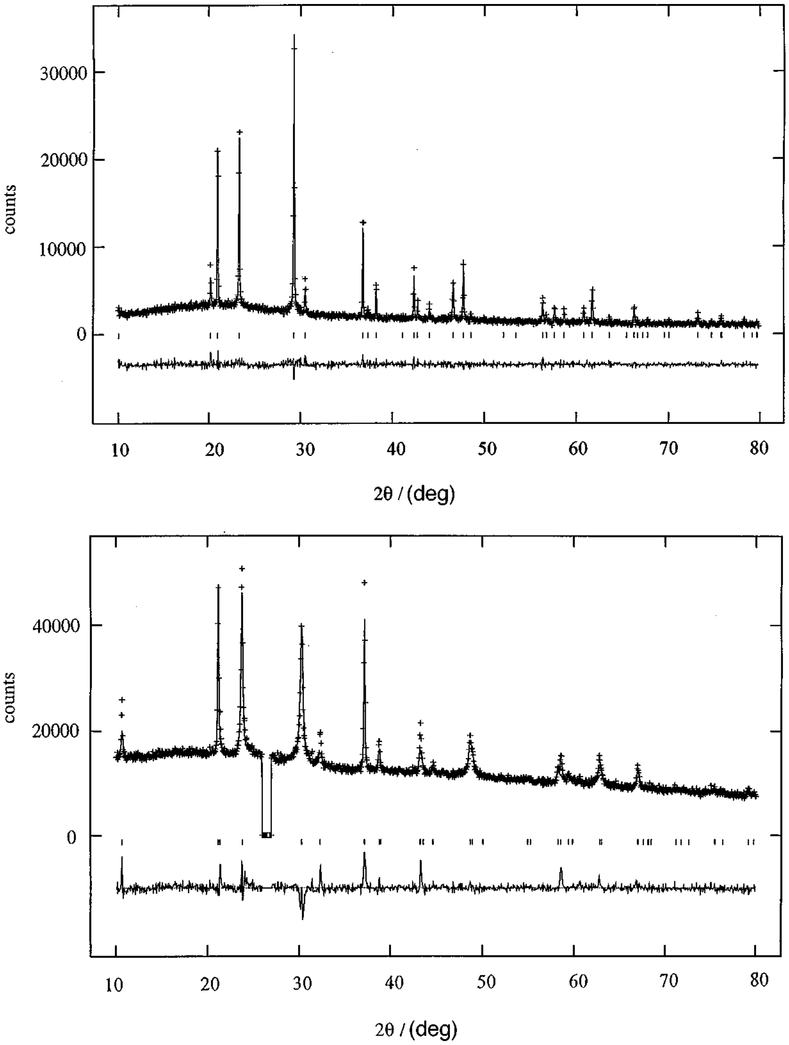

FIG. 2. X-ray powder diffractograms (Cu $K\alpha_1$ radiation) at ambient temperature (a) for $CsFe(SO_4)_2$ (agreement factors $R_p = 0.063$, $R_{wp} = 0.081$) and (b) for $RbFe(SO_4)_2$ (agreement factors $R_p = 0.035$, $R_{wp} = 0.052$). The plots show experimental intensity (+), calculated intensity (upper solid line), and difference intensity (observed and calculated, lower solid line). In (b) there are excluded peaks at $2\theta = 26.2°$, $2\theta = 26.6°$ believed to arise from an unknown impurity. A shoulder at 24.5°, also believed to arise from the impurity, is not excluded.

the diffractogram recorded above the Néel temperature from the diffractogram recorded below the Néel temperature. The scale factors for data recorded above and below the Néel temperature were assumed to be the same. Invoking these approximations allowed a reliable value of the magnetic moment to be determined (note that the value of the magnetic moment is correlated with the scale factor). No symmetry was assumed for the magnetic structure, and the space group $P1$ was therefore used. The magnetic form factor for Fe^{3+} was calculated from Ref. 21. The line shape was taken as pseudo-Voigt, and the zero-point correction parameter was taken as the value refined for the low-temperature nuclear structure at 20 K for $CsFe(SO_4)_2$ and 8 K for $RbFe(SO_4)_2$. For Rietveld refinement of the magnetic structure, the program GSAS (Ref. 22) was used to test commensurate models, and the program FULLPROF (Ref. 23) was used to test incommensurate models, as described below.

C. Crystal structures of $CsFe(SO_4)_2$ and $RbFe(SO_4)_2$

The synchrotron x-ray powder diffractograms were indexed using the program ITO,[24] leading to cells with trigonal metric symmetry for both $CsFe(SO_4)_2$ and $RbFe(SO_4)_2$. As mentioned in Sec. I, the $AM(XO_4)_2$ phases characterized so far can be classified according to six structure types. Three of these are trigonal and are typified by $KAl(MoO_4)_2$ ($P\overline{3}m1$, $a = 5.545$ Å, $c = 7.070$ Å),[25] $KAl(SO_4)_2$ ($P321$, $a = 4.71$ Å, $c = 8.01$ Å),[26] and $CsSb(PO_4)_2$ ($P\overline{3}$, $a = 4.825$ Å, $c = 9.226$ Å).[16] Initially, all three structure types were considered as possible models for $CsFe(SO_4)_2$ and $RbFe(SO_4)_2$, as the three space groups cannot be distinguished on the basis of systematic absences. Each structure type has one layer per unit cell. The A and M cations are in special positions which alternate along the c axis, and the X atom and one O atom of the XO_4 units are also in special positions. The main difference between the three structure types concerns the degree of rotation of the XO_4 units around an axis perpendicular to the layers. The complete set of atomic positions is characterized by five coordinates, and only these coordinates and isotropic atomic displacement parameters were refined.

For $CsFe(SO_4)_2$ at ambient temperature, structure refinement (using x-ray powder diffraction data) based on the $CsSb(PO_4)_2$ structure[16] gave a better description than the other two structure types. The refined structural parameters are reported in Table II(a), and the experimental and calculated powder diffractograms are compared in Fig. 2(a).

The low-temperature (20 K) nuclear structure of $CsFe(SO_4)_2$ was refined from the neutron powder diffraction data using the crystal structure determined at ambient temperature as the starting point. The final refined structural parameters are reported in Table II(b).

Refinement of the crystal structure for $RbFe(SO_4)_2$ at ambient temperature (x-ray powder diffraction data) based on the $CsSb(PO_4)_2$ structure[16] also gave better agreement than the other two structure types. The final refined structural parameters are reported in Table II(c), and the fitted powder diffraction profile is shown in Fig. 2(b). Excluded from this refinement are two weak Bragg peaks at $2\theta=26.2°$ and $2\theta=26.6°$ which arise from an unidentified impurity in the sample. The latter also gives rise to a shoulder at $2\theta=24.5°$ which was not excluded. The peaks were assigned to the impurity on the grounds that (a) not all samples contain them, (b) their relative intensities are always similar, and (c) the other Bragg peak intensities and shapes do not depend upon their presence or absence. The samples used for the diffraction experiments were preferred on the grounds of their relatively good crystallinity, despite containing a small amount of this impurity. Comparison of several samples showed that the contribution to the diffraction profile of all peaks arising from the impurity, with the exception of those mentioned above, could be safely neglected.

The low-temperature (8 K) nuclear structure of $RbFe(SO_4)_2$ was refined (for the neutron powder diffraction data) using the crystal structure at ambient temperature as the starting point. The final refined structural parameters are reported in Table II(d). In the low-temperature neutron powder diffraction profile for $RbFe(SO_4)_2$, some of the Bragg peaks are perceptibly broader than the others, and a good fit of all peaks in the diffractogram can be obtained only by assigning the peaks to two subsets and considering different line profile parameters for each subset. We are currently investigating the physical origin of this effect using a number of approaches, including consideration of higher-resolution neutron powder diffraction data.

The crystal structures of $CsFe(SO_4)_2$ and $RbFe(SO_4)_2$ are illustrated in Fig. 3. They differ mainly in terms of the repeat distance along the c axis, which is significantly greater for $CsFe(SO_4)_2$, presumably as a result of the larger ionic radius for Cs than Rb. For both $CsFe(SO_4)_2$ and $RbFe(SO_4)_2$, the crystal structure at low temperature is essentially the same as the crystal structure at ambient temperature, except for the expected lattice contraction upon cooling.

D. Indexing of the magnetic diffraction pattern and definition of magnetic models

The neutron powder diffractograms recorded at 1.3 K contain peaks that arise from three-dimensional magnetic order. The magnetic diffraction patterns (difference diffractograms) of $CsFe(SO_4)_2$ and $RbFe(SO_4)_2$ are different, but can both be indexed by the following magnetic cell: $a_m=b_m=a\sqrt{3}$, $c_m=2c$, $\alpha_m=\beta_m=90°$, and $\gamma_m=60°$, where a, b, and c denote the nuclear cell parameters.

We found it appropriate to consider two magnetic models, which are consistent with this magnetic cell. These models are illustrated in Figs. 4(a)–4(d) and described below.

1. Model C1 (commensurate 1)

In this model the atomic magnetic moments form a three-sublattice structure within the a_mb_m (basal) plane, with adjacent moments rotated by 120° with respect to their neighbors [Fig. 4(a)]. The stacking of the moments along the c_m axis is antiferromagnetic [Fig. 4(b)]. The magnetic space group is P_c3.[27]

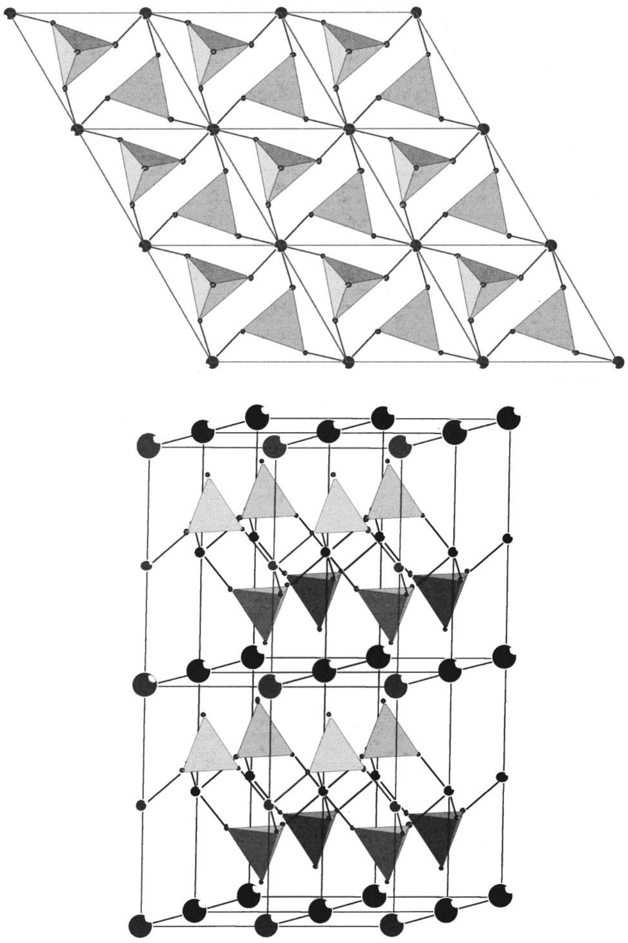

FIG. 3. Representations of the crystal structure of $CsFe(SO_4)_2$, showing sulfate tetrahedra, Fe^{3+} ions (medium black circles), and Cs^+ ions (large black circles): (a) looking down the c axis and (b) looking approximately along the a axis. Except for minor differences the crystal structure of $RbFe(SO_4)_2$ is the same as that of $CsFe(SO_4)_2$ (with Cs replaced by Rb).

2. Model C2 (commensurate 2)

This model differs from the model $C1$ in that the angle ϕ between the orientations of adjacent spins in directions parallel to the c_m takes a value different to the antiferromagnetic value $\phi=180°$ [Fig. 4(c)]. The magnetic space group is $P3$.[27]

We have also given consideration to the following incommensurate magnetic model.

3. Model I1 (incommensurate 1)

This magnetic model has a 120° structure in the basal plane [Fig. 4(a)] and an incommensurate relationship between the periodicities of the magnetic and nuclear structures along the c_m axis [Fig. 4(d)]. Although we observed no evidence for satellite peaks in the neutron powder diffraction patterns of either $CsFe(SO_4)_2$ or $RbFe(SO_4)_2$, they may have been obscured by the relatively low resolution of the instru-

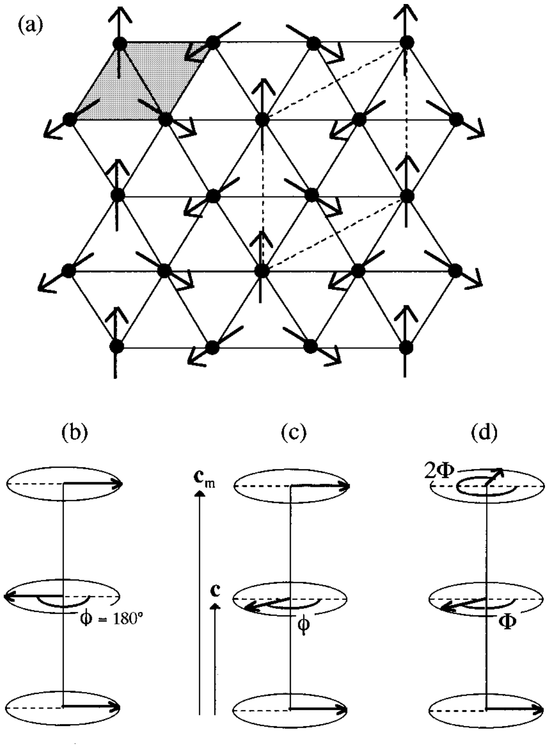

FIG. 4. Magnetic structure models $C1$, $C2$, and $I1$ discussed in the text: (a) Spin structure in the a-b (basal) plane common to all three models. The figure shows the crystallographic unit cell (shaded parallelogram) and magnetic unit cell (dashed line). The atomic magnetic moments (arrows) lie in the basal plane, with the orientation of adjacent moments rotated by 120°. The figure shows only one possible spin configuration, as all others related by a global rotation of the spins through an arbitrary angle within the a-b plane give rise to the same powder neutron diffraction pattern and hence cannot be distinguished experimentally for $CsFe(SO_4)_2$ and $RbFe(SO_4)_2$. (b) Spin structure along the c axis for model $C1$ (commensurate 1), defining the angle ϕ discussed in the text, which for model $C1$ is restricted to the antiferromagnetic value 180°. (c) Spin structure along the c axis for model $C2$ (commensurate 2), in which the angle ϕ can take any value. Also shown is the relationship between the vector **c** of the crystallographic unit cell and the vector $\mathbf{c}_m$ of the magnetic unit cell for models $C1$ and $C2$. (d) Spin structure along the c axis for model $I1$ (incommensurate 1), defining the angle Φ discussed in the text.

ment. An incommensurate model, with a modulation angle close to 180°, is thus consistent with the indexing described above. The magnetic peaks are indexed by a propagation vector $\mathbf{k}=[1/3\,1/3\pm\delta]$, where the components are referred to the reciprocal lattice vectors corresponding to the nuclear structure, and the modulation angle between the spins in adjacent basal planes is given by $\Phi=\delta\times 360°$ [see Fig. 4(d)].

E. Magnetic structures of $CsFe(SO_4)_2$ and $RbFe(SO_4)_2$

The three magnetic models $C1$, $C2$, and $I1$ described above were considered for both $CsFe(SO_4)_2$ and $RbFe(SO_4)_2$. The fits of these theoretical models to the difference diffractograms are illustrated in Figs. 5(a)–5(e).

The antiferromagnetic ($\phi=180°$) model $C1$ was considered first. In order to ensure stability in the refinement, the magnetic moment was not refined, but was fixed in any given calculation. Different calculations were carried out for different (fixed) values of the magnetic moment. For $CsFe(SO_4)_2$ the best agreement factors ($R_{wp}=0.058$, $R_p=0.040$) were obtained for $\mu=4.2\mu_B$, with an estimated error in μ of $\pm 0.2\mu_B$. The good agreement between the experimental and calculated neutron powder diffractograms is shown in Fig. 5(a). If the angle ϕ between the orientation of adjacent magnetic moments in directions parallel to the c axis was changed from 180° (model $C2$), a significantly worse fit to the magnetic diffraction data was obtained for ϕ outside the range $180°\pm 10°$. Thus we can conclude that the coupling along the c axis is antiferromagnetic or very close to antiferromagnetic.

For $RbFe(SO_4)_2$ reasonable agreement factors for model CI were obtained for $\mu=4.5\mu_B$. The experimental and calculated diffractograms are compared ($R_{wp}=0.089$, $R_p=0.062$) in Fig. 5(b). The agreement is moderately good, although there is no significant intensity in the calculated diffractogram for the peak that represents the superposition of the reflections within the form {1,0,0} at $2\theta=19.73°$. It should be noted that, first, the magnetic reflections are indexed on the magnetic cell, and second, these reflections occur at the same 2θ value, as a consequence of the trigonal metric symmetry, but the individual reflections [e.g., (1,0,0), (1,1,0), (0,1,0)] within the {1,0,0} form are not constrained to have the same intensities, as a consequence of assuming the space group $P1$. The observation of this Bragg peak means that the projection of the magnetic moments on at least one of the (100), (110), and (010) planes is nonzero. A component can be introduced in these planes (leading to increased intensity of the {100} peak) by assuming model $C2$, in which ϕ differs from 180°. However, on decreasing the value of ϕ, other peaks also become more intense (such as the peak representing the superposition of the reflections within the form {1,0,2} at $2\theta=26.83°$, which has low intensity in the experimental diffractogram). The overall best fit is achieved by a compromise in terms of fitting these two sets of peaks. The optimum value of ϕ was determined to be $150°\pm 10°$ [Fig. 5(c)], corresponding to agreement factors $R_{wp}=0.078$, $R_p=0.051$, and $\mu=4.5\mu_B$.

The incommensurate model $I1$ was also tested for both materials. In fitting this model to the data, the refined parameters were the value of δ (defined in Sec. IV D) and the magnitude of the magnetic moment μ. For $CsFe(SO_4)_2$ the final refined value of $\delta=0.457(2)$ corresponds to a modulation angle Φ between adjacent basal planes of approximately 165°, and the final refined value of the magnetic moment is $\mu=4.5\mu_B$ (with an estimated error of $0.2\mu_B$); the observed and calculated diffractograms are shown in Fig. 5(d). The agreement factors for this refinement are $R_p=0.060$ and $R_{wp}=0.080$. The discrepancies between the experimental and calculated diffractograms are slightly larger for this model than for the model $C1$ (which has antiferromagnetic coupling along the c axis), although on the basis of the quality of data presently available, the incommensurate model certainly cannot be ruled out.

In considering model $I1$ for $RbFe(SO_4)_2$, the refined value of $\delta=0.462(2)$ corresponds, as for $CsFe(SO_4)_2$, to a modulation angle of approximately 165°. The refined value of the magnetic moment was $\mu=4.8\mu_B$ (with estimated error

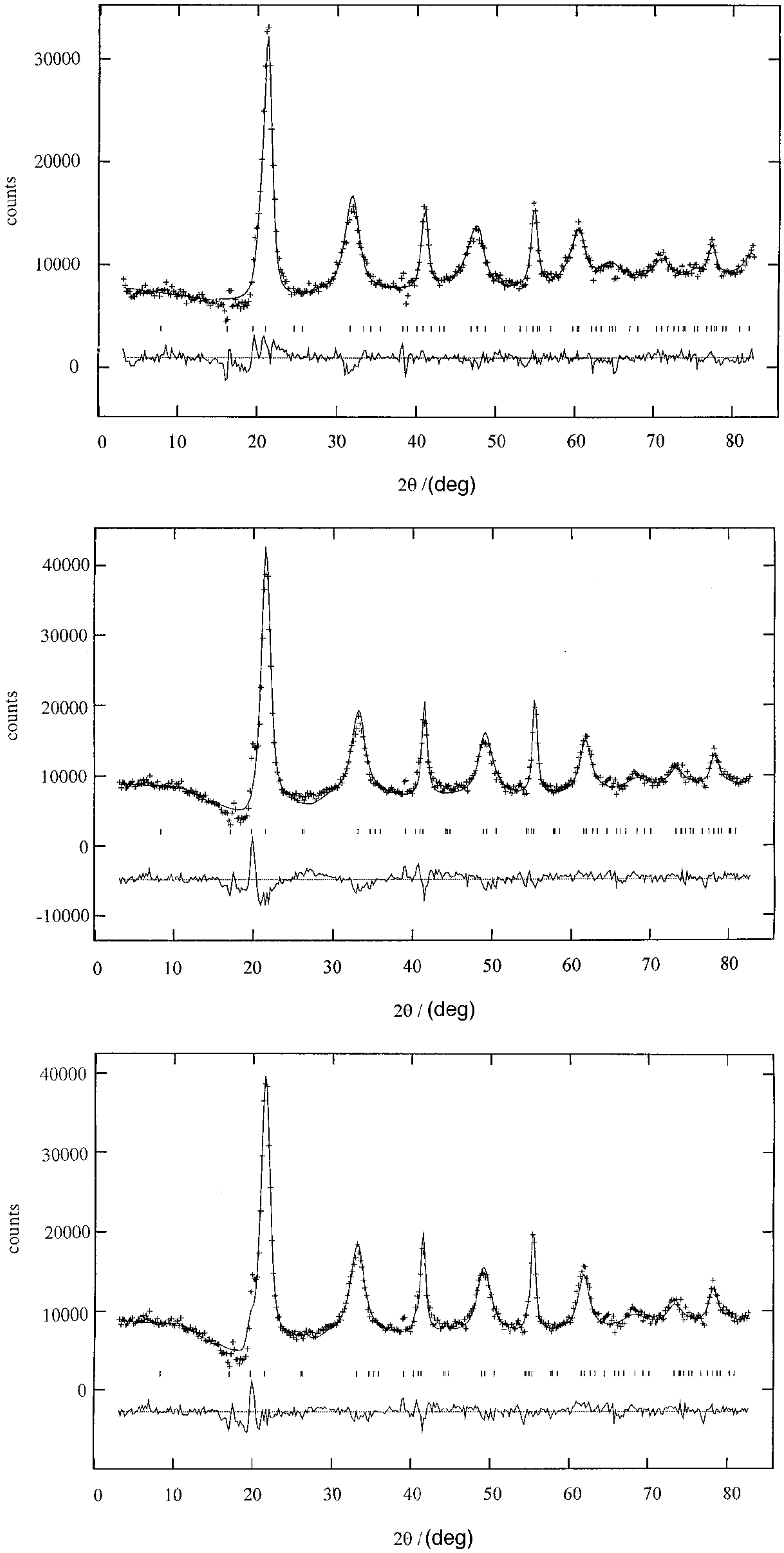

FIG. 5. Fits of magnetic models $C1$, $C2$, and $I1$ (defined in Fig. 4) to experimental magnetic powder diffraction patterns at 1.3 K. The figures show experimental (+), calculated (upper solid line), and difference (observed and calculated, lower solid line) magnetic diffraction profiles. The experimental profile was obtained by subtracting the neutron powder diffraction pattern recorded above the magnetic ordering temperature, from the neutron powder diffraction pattern recorded below the magnetic ordering temperature, as described in the text: The error in the magnetic moment μ is estimated to be $\pm 0.2\mu_B$ in each case. (a) Test of model $C1$ for $CsFe(SO_4)_2$ at 1.3 K. ($\mu = 4.2\mu_B$, $R_p = 0.040$, $R_{wp} = 0.058$). (b) Test of model $C1$ for $RbFe(SO_4)_2$ ($\mu = 4.5\mu_B$, $R_p = 0.062$, $R_{wp} = 0.089$). (c) Test of model $C2$ for $RbFe(SO_4)_2$ [$\mu = 4.5\mu_B$, $\phi = 150° \pm 10°$, $R_p = 0.051$, $R_{wp} = 0.078$). (d) Test of model $I1$ for $CsFe(SO_4)_2$ ($\mu = 4.5\mu_B$, $\delta = 0.457(2)$, $\Phi \approx 165°$, $R_p = 0.060$, $R_{wp} = 0.080$]. (e) Test of model $I2$ for $RbFe(SO_4)_2$ [$\mu = 4.8\mu_B$, $\delta = 0.462(2)$, $\Phi \approx 165°$, $R_p = 0.075$, $R_{wp} = 0.105$].

$0.2\mu_B$), and the observed and calculated diffractograms are shown in Fig. 5(e) (agreement factors $R_p = 0.075$ and $R_{wp} = 0.105$). Again, the agreement is reasonably good, although it should be noted that this model does not predict any reflection at the experimentally observed position $2\theta = 19.73°$. Again, on the basis of the quality of data presently available, the incommensurate model cannot be ruled out for $RbFe(SO_4)_2$.

Thus, in the magnetic structures refined for $CsFe(SO_4)_2$ and $RbFe(SO_4)_2$, the magnetic moments form a ''120°'' structure in the basal plane. The balance of evidence is in favor of a model in which there are two basal planes in the periodic repeat distance of the magnetic structure along the c_m axis; however, an incommensurate model cannot be ruled out. Assuming the commensurate model, the relative orientations of adjacent magnetic moments in directions parallel

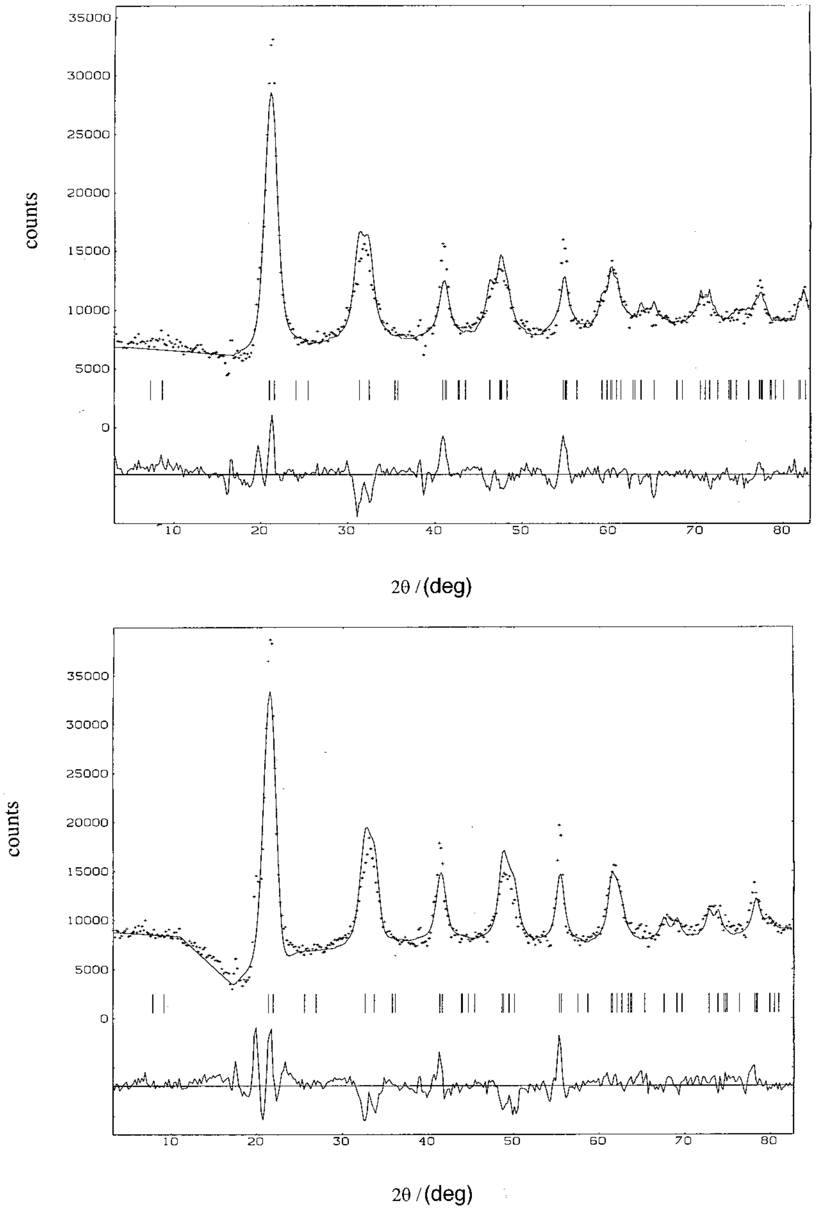

FIG. 5. (*Continued*).

to the c_m axis differ by about for 180° [$CsFe(SO_4)_2$] and about 150° [$RbFe(SO_4)_2$]. It is important to note that the orientation of the spins with respect to the a_m and b_m axes cannot be determined from neutron powder diffraction data.[28] Corresponding models were also considered in which the magnetic moments lie out of the basal planes; however, the agreement was significantly worse for these models than for the models (discussed above) with the magnetic moments constrained to lie in the basal planes. Similar models to those determined here for $CsFe(SO_4)_2$ and $RbFe(SO_4)_2$ have been used to describe the magnetic structure of $CsMnBr_3$.[29]

V. CONCLUDING REMARKS

We have shown that $CsFe(SO_4)_2$ and $RbFe(SO_4)_2$ both approximate very well the two-dimensional Heisenberg model antiferromagnet on the triangular lattice. Their ordered magnetic structures consist of a three-sublattice structure in the basal plane, with adjacent spins rotated by 120°, which is similar to the spin structure of $CsMnBr_3$.[29] At 1.3 K the refined value of the magnetic moment is close to 5, the expected spin-only moment for Fe^{3+}. The result that the atomic magnetic moments lie within the basal planes suggests that there may be weak *XY* anisotropy in the spin Hamiltonian which forces the spins into the a-b plane of the crystal structure. It has been proposed[30] that $CsFe(SO_4)_2$ has weak Ising-like single ion anisotropy; however, the site symmetry at the Fe^{3+} sites is $\overline{3}$, which means that Ising anisotropy cannot force the spins into the basal plane. For both $CsFe(SO_4)_2$ and $RbFe(SO_4)_2$, the stacking of the magnetic structure along the c axis is close to antiferromagnetic, but we cannot rule out an incommensurate model in either case. In a recent publication,[30] Inami *et al.* refer to a preliminary unpublished neutron diffraction study which suggests that $CsFe(SO_4)_2$ is indeed described by our incommensurate model *I*1. In order to make a definitive comparison between the commensurate and incommensurate models of the magnetic structures of $CsFe(SO_4)_2$ and $RbFe(SO_4)_2$, neutron powder diffraction data recorded with higher instrumental resolution are required.

[*] Authors to whom correspondence should be addressed.

[1] For reviews, see J. M. D. Coey, Can. J. Phys. **65**, 1210 (1987); in *Magnetic Systems with Competing Interactions*, edited by H. T. Diep (World Scientific, Singapore, 1994); E. F. Shender and P. C. W. Holdsworth, in *Fluctuations and Order: A New Synthesis*, edited by M. M. Millonas (Springer-Verlag, Berlin, 1996).

[2] K. Kawamura and S. Miyashita, J. Phys. Soc. Jpn. **53**, 4138 (1984); S. Miyashita, *ibid.* **55**, 3605 (1986); S. Miyashita and H. Shiba, *ibid.* **53**, 1145 (1984); S. Miyashita and H. Kawamura, *ibid.* **54**, 3385 (1985).

[3] H. Kawamura, Phys. Rev. B **47**, 3415 (1993).

[4] P. W. Anderson, Mater. Res. Bull. **8**, 153 (1973).

[5] A. Harrison and T. E. Mason, J. Appl. Phys. **67**, 5424 (1990).

[6] G. Wannier, Phys. Rev. **79**, 357 (1950).

[7] P. W. Anderson, Science **235**, 1196 (1987).

[8] D. A. Huse and V. Elser, Phys. Rev. Lett. **60**, 2531 (1988); N. Elstner, R. R. P. Singh, and A. P. Young, *ibid.* **71**, 1629 (1993).

[9] K. Hirakawa, H. Ikeda, H. Kadowaki, and K. Ubukoshi, J. Phys. Soc. Jpn. **52**, 2882 (1983).

[10] H. Kadowaki, H. Kikuchi, and Y. Ajiro, J. Phys.: Condens. Matter **5**, 4225 (1993).

[11] D. Visser and A. Harrison, J. Magn. Magn. Mater. **116**, 80 (1992).

[12] O. A. Petrenko, M. F. Collins, C. V. Stager, B. F. Collier, and Z. Tun, J. Appl. Phys. **79**, 6614 (1996).

[13] K. Hirakawa, H. Kadowaki, and K. Ubukoshi, J. Phys. Soc. Jpn. **54**, 3526 (1985).

[14] J. N. Reimers, J. R. Dahn, J. E. Greedan, C. V. Stager, G. Liu, I. Davidson, and U. Von Sacken, J. Solid State Chem. **102**, 542 (1993).

[15] S. T. Bramwell, S. G. Carling, C. J. Harding, K. D. M. Harris, B. M. Kariuki, L. Nixon, and I. P. Parkin, J. Phys.: Condens. Matter **8**, L123 (1996).

[16] S. Oyatola, A. Verbaere, Y. Piffard, and M. Tournoux, Eur. J. Solid State Inorg. Chem. **25**, 259 (1988), and references therein.

[17] H. Kawamura, Prog. Theor. Phys. Suppl. **101**, 545 (1990); W. M. Zhang, W. M. Saslow, and M. Gabay, Phys. Rev. B **44**, 5129 (1991); W. M. Zhang, W. M. Saslow, M. Gabay, and M. Benakli, *ibid.* **48**, 10 204 (1993); M. E. Zhitomirsky, *ibid.* **54**, 353 (1996).

[18] J. Bernard and J.-P. Couchot, C. R. Seances Acad. Sci., Ser. C **262**, 209 (1966).

[19] H. Ikeda and K. Hiwakawa, Solid State Commun. **14**, 529 (1974).

[20] S. T. Bramwell and P. C. W. Holdsworth, J. Phys.: Condens. Matter **5**, L53 (1993).

[21] E. J. Lisher and J. B. Forsyth, Acta Crystallogr., Sect. A: Cryst. Phys., Diffr., Theor. Gen. Crystallogr. **27**, 545 (1971).

[22] A. C. Larson and R. B. Von Dreele (unpublished).

[23] J. Rodriguez-Carvajal, computer code FULLPROF, 1990.

[24] J. W. Visser, J. Appl. Crystallogr. **2**, 89 (1961).

[25] R. F. Klevtsova and P. V. Klevtsov, Kristallografiya **15**, 953 (1970) [Sov. Phys. Crystallogr. **15**, 829 (1971)].

[26] J. M. Manoli, P. Herpin, and G. Pannetier, Bull. Soc. Chim. Fr. **1**, 98 (1970).

[27] N. V. Belov, N. N. Neronova, and T. S. Smirnova, Sov. Phys. Crystallogr. **2**, 311 (1957).

[28] G. Shirane, Acta Crystallogr. **12**, 282 (1959).

[29] M. Eibshutz, R. C. Sherwood, F. S. L. Hsu, and D. E. Cox, in *Magnetism and Magnetic Materials*, edited by C. D. Graham, Jr. and J. J. Rhyne, AIP Conf. Proc. No. 10 (AIP, New York, 1973), p. 684.

[30] T. Inami, Y. Ajiro, and T. Goto, J. Phys. Soc. Jpn. **65**, 2374 (1996).